

An Adaptive Volumetric Flux Boundary Condition for Lattice Boltzmann Methods

James E. McClure¹, Zhe Li², Adrian P. Sheppard², Cass T. Miller³

Abstract

This paper presents a spatially and temporally adaptive boundary condition to specify the volumetric flux for lattice Boltzmann methods. The approach differs from standard velocity boundary conditions because it allows the velocity to vary over the boundary region provided that the total flux through the boundary satisfies a prescribed constraint, which is a typical scenario for laboratory experimental studies. This condition allows the boundary pressure to adjust dynamically to yield a specified boundary flow rate as a means to avoid unphysical mismatch between the boundary velocity and the interior flow field that can arise when a constant velocity boundary condition is applied. The method is validated for simulation of one- and two-fluid flow in complex materials, with conditions determined to match typical experiments used to study flow in porous media.

Keywords: velocity boundary condition, pressure boundary condition

2010 MSC: 00-01, 99-00

1. Introduction

It is often desirable to design computational protocols that match particular experimental conditions. Setting appropriate boundary conditions is an

Email address: mccurej@vt.edu (James E. McClure)

¹Advanced Research Computing, Virginia Tech, Blacksburg, USA.

²Department of Applied Mathematics, Australia National University, Canberra, ACT 2601, Australia

³University of North Carolina at Chapel Hill

important aspect of this endeavor. In computational methods, artificial boundary conditions are routinely imposed as a way to focus computational effort on a particular region of interest [1]. Lattice Boltzmann methods (LBMs) are a broad class of computational methods that are used widely to study complex fluid flows [2, 3, 4, 5, 6, 7, 8]. Boundary conditions for the LBM differ from standard Neumann and Dirichlet boundary conditions used for partial differential equations (PDEs) because of the way that LBMs are constructed. The LBM originates as a discrete form of the Boltzmann equation, and the number of unknown quantities at the boundary is determined by this choice. Boundary conditions must determine each unknown distribution, with the total number of unknowns determined by the discrete velocity structure and boundary shape. Commonly used boundary conditions for LBMs include pressure, velocity, periodic and outflow boundary conditions [9, 10]. For experimental studies of flows in porous media, microfluidics, and other complex materials, it is common to monitor (or to control directly) the total volumetric injection rate into the system. To be specific, we will call this common volumetric flux boundary condition a macroscale condition since it is an integrated quantity applied on the boundary. The common alternative conditions are microscale conditions because these conditions prescribe point-wise values of fluid velocities or pressures at the microscale, or lattice scale. Under such conditions, the microscale velocity profile at the boundary will be known only on rare occasions. Velocity boundary conditions that are inconsistent with the interior flow present a particular challenge, since such conditions are a source of physical inaccuracy.

When setting velocity boundary conditions, inaccuracy can result if the condition assigned leads to a rapid change in flow conditions near the boundary region. In particular, large gradients in an underlying potential field may result. Since potential gradients induce flow, spurious behavior can arise to correct artifacts in the potential field. Since the potential and velocity cannot be independently determined, a velocity boundary condition can lead to direct enforcement of potential gradients along the boundary. When the potential is determined implicitly, flow may be inconsistent with the local potential field. Setting constant

microscale potential boundary conditions (e.g. a pressure boundary condition) is simpler and often more physically reasonable. However, in this scenario, the macroscale boundary flow rate is determined as a result of the microscale system dynamics, and cannot be prescribed using established approaches. We consider the case where the total macroscale volumetric flux through a particular boundary is specified, and seek a boundary condition consistent with this condition.

Thus, the overall goal of this work is to derive a macroscale flux boundary condition that applies to the LBM simulation of flow through porous media that is stable and efficient. The specific objectives of this paper are (1) to formulate a general boundary condition to control the volumetric flux in lattice Boltzmann methods; (2) to validate the numerical approach based on analytical results; and (3) to apply the method to match experimental conditions for single-fluid and two-fluid flows.

2. Methods

LBM is a computationally efficient class of numerical method that are widely used to model flows in complex geometries. Inspired by kinetic theory, LBMs solve for the evolution of a fluid flow by considering a set of distributions f_q , each associated with a discrete velocity ξ_q with $q \in \{0, 1, \dots, Q\}$. Subject to constraints on symmetry and Galilean invariance, LBMs have been developed using various different discrete velocity sets to model flows in two (e.g. D2Q9) or three dimensions (e.g. D3Q13, D3Q15, D3Q19, D3Q27) [11, 12, 13, 14]. In this work, we present a volumetric flux boundary condition for the popular D3Q19 model. The same general principles can be used to derive analogous boundary conditions for other models. In the D3Q19 model, the set of discrete

velocities are

$$\xi_q = \begin{cases} \{0, 0, 0\}^T & \text{for } q = 0 \\ \{\pm 1, 0, 0\}^T, & \text{for } q = 1, 2 \\ \{0, \pm 1, 0\}^T, & \text{for } q = 3, 4 \\ \{0, 0, \pm 1\}^T & \text{for } q = 5, 6 \\ \{\pm 1, \pm 1, 0\}^T, & \text{for } q = 7, 8, 9, 10 \\ \{\pm 1, 0, \pm 1\}^T, & \text{for } q = 11, 12, 13, 14 \\ \{0, \pm 1, \pm 1\}^T & \text{for } q = 15, 16, 17, 18. \end{cases} \quad (1)$$

The distributions evolve according to the lattice Boltzmann equation

$$f_q(\mathbf{x}_i + \boldsymbol{\xi}_q \delta t, t + \delta t) = f_q(\mathbf{x}_i, t) + \Omega_q(\mathbf{x}_i, t), \quad (2)$$

where \mathbf{x}_i are points on a three-dimensional lattice, $i \in \{0, 1, \dots, N\}$, δt is the time step, and $\Omega_q(\mathbf{x}_i, t)$ is a collision operator that accounts for intermolecular collisions and other interactions (as in Boltzmann’s equation). The key physics of the method are contained in the collision operation. By constructing different collision operators, LBMs have been constructed to recover the Navier-Stokes equations [15, 16] and model a wide range of physical processes including multi-phase flow [17, 18, 19, 20, 21], heat transfer [22, 23, 24, 25], diffusion [26, 27, 28], reactive transport [29, 30, 31] and others. Since the basic approaches used to set boundary conditions are similar, the boundary condition developed here can be extended to other physical contexts as well.

In this work, an adapted multi-relaxation time (MRT) LB model is implemented for single-/two-fluid flow as described in McClure *et al.* [32], which is based on the “color” model initially proposed by Gustensen *et al.* [17]. More details of the model can be found in [Appendix A](#). In short, an MRT formulation for a DdQq lattice structure models the relaxation processes individually on a set of q moments determined from the distributions, where each moment relaxes toward its equilibrium value at a unique rate specified by relaxation parameters. Following the previous work by Pan *et al.* [33], the fluid kinematic viscosity ν is related to one of the relaxation parameter τ by $\nu = c_s^2(\tau - 0.5)$, where c_s is the

LBM speed of sound. Other relaxation parameters can be found in [Appendix A](#).

The interpretation of the distributions is key to constructing LBMs to model different physical phenomena. Based on this, moments of the distributions track the behavior of physical quantities of interest. Often the distributions are defined to determine the evolution of the number density,

$$\rho = \sum_{q=0}^{Q-1} f_q, \quad (3)$$

and the mass flux (momentum density),

$$\mathbf{j} = \rho_0 \mathbf{u} = \sum_{q=0}^{Q-1} f_q \boldsymbol{\xi}_q, \quad (4)$$

where ρ_0 is a reference density used to obtain incompressible flow. This represents a typical LBM formulation, although distributions may also be defined to track other physical quantities of interest. In the LBM, the pressure is often directly linked to the density,

$$p = c_s^2 \rho, \quad (5)$$

which is an expression of the ideal gas law. Boundary conditions are needed to determine unknown distributions along the boundary, which in turn determine the density ρ and momentum density $\rho_0 \mathbf{u}$.

The most familiar context for fluid flow simulations is to set pressure and/or velocity boundary conditions. The basic ideas used to set pressure or velocity boundary conditions for LBMs were first introduced by Zou and He for the D2Q9 model [34]. Along a boundary region Γ , only a subset of the distributions will be unknown. For some $\mathbf{x}_i \in \Gamma$, distributions f_q are unknown for all q such that $\mathbf{x}_i - \boldsymbol{\xi}_q \delta t \notin D$, where D is the domain. At the inlet, the unknown distributions are: $f_5, f_{11}, f_{14}, f_{15}$ and f_{18} . Three of the unknown distributions can be determined based on Eqs. 3–4. As a consequence of the continuity equation, it is not possible to set both ρ and u_z along the z inlet or outlet. When setting a pressure (i.e. density) boundary condition at the z inlet, a

consistency condition establishes the associated velocity u_z as a function of the known distributions and density

$$u_z = \frac{\rho}{\rho_0} - \frac{1}{\rho_0} \left[f_0 + f_1 + f_2 + f_3 + f_4 + f_7 + f_8 + f_9 + f_{10} + 2(f_6 + f_{12} + f_{13} + f_{16} + f_{17}) \right]. \quad (6)$$

The consistency condition will be used to derive an adaptive pressure boundary condition that satisfies a specified macroscale boundary volumetric flux.

In this work, we seek to specify the total volumetric flux across the boundary, which is defined as

$$Q_z = \int_{\Gamma_{in}} u_z dr, \quad (7)$$

where Γ_{in} is the inlet boundary. We note that at each microscale point on the boundary u_z can be determined prior to setting the pressure boundary condition based on the consistency condition. Combining Eq. 6 with Eq. 7 we obtain

$$Q_z = \int_{\Gamma_{in}} \frac{\rho}{\rho_0} - \frac{1}{\rho_0} \left[f_0 + f_1 + f_2 + f_3 + f_4 + f_7 + f_8 + f_9 + f_{10} + 2(f_6 + f_{12} + f_{13} + f_{16} + f_{17}) \right] dr. \quad (8)$$

Our objective is to determine the value of ρ that will produce a user-specified Q_z , where ρ is constant over the boundary Γ_{in} . The expression can be rearranged to solve for ρ in terms of the known distributions on Γ_{in}

$$\rho = \frac{\rho_0 Q_z}{A} + \frac{1}{A} \int_{\Gamma_{in}} \left[f_0 + f_1 + f_2 + f_3 + f_4 + f_7 + f_8 + f_9 + f_{10} + 2(f_6 + f_{12} + f_{13} + f_{16} + f_{17}) \right] dr, \quad (9)$$

where A is the area of the inlet. Integrating the consistency condition over the boundary thereby determines ρ . As with other boundary conditions for the LBM, the condition must be applied after streaming and prior to collision. At each timestep, the boundary condition is set in two steps; first ρ is determined by integrating the consistency condition according to Eq. 9, then a pressure boundary condition is enforced in the usual way based on Eqs. 5 and 9. For the pressure boundary condition, the strategy to determine the remaining two

unknowns for the D3Q19 model is based on the work due to Hecht and Harting [35] (see more details in Appendix B). An analogous calculation can be performed at the outlet boundary, although it is not necessary or advantageous to set a flux boundary condition at both boundaries. Since the potential field is in general only known up to a constant, it is convenient to set a flux boundary condition at one end of the sample and rely on a pressure boundary condition at the other end of the domain, where the other four boundaries can be assigned using periodic or no flow conditions. We have constrained our case to match typical experimental conditions, but the notions can be extended to other sorts of systems as well.

3. Results

3.1. Single-phase Poiseuille flow

In this section, to verify the accuracy of the proposed macroscale volumetric flux boundary condition, a three-dimensional (3D) Poiseuille flow simulation in a square tube of size $(L_x, L_y, L_z) = (40, 40, 80)$ is performed. The discrete unit of the computational grid is a lattice unit (lu), and the iteration of the LB simulation is in the unit of lattice time (lt). The flow direction is along the z -axis. For a square tube, if the Cartesian origin is at the center of the plane normal to the flow axis, and the flow region is: $-w \leq x \leq w$ and $-w \leq y \leq w$, the 3D Poiseuille flow is known to have a steady-state solution given by [36]:

$$u_z(x, y) = \frac{16a^2}{\nu\pi^3} \left(-\frac{dp}{dz} \right) \sum_{k=1,3,5,\dots}^{\infty} (-1)^{(k-1)/2} \left\{ 1 - \frac{\cosh[k\pi x/(2w)]}{\cosh(k\pi/2)} \right\} \frac{\cos[k\pi y/(2w)]}{k^3}, \quad (10)$$

where w is half of the width of the square tube, dp/dz is the pressure gradient along the flow axis of the tube, and ν is the kinematic viscosity of the fluid. The infinite series in Eq.10 was truncated at $k = 200$ to allow for a good approximation of the theoretical values. For the numerical simulations, the criterion used to determine steady state flow is

$$\frac{\sum_{\mathbf{x}} |\mathbf{u}(\mathbf{x}, t) - \mathbf{u}(\mathbf{x}, t - 1000)|}{\sum_{\mathbf{x}} |\mathbf{u}(\mathbf{x}, t)|} \leq 10^{-6}. \quad (11)$$

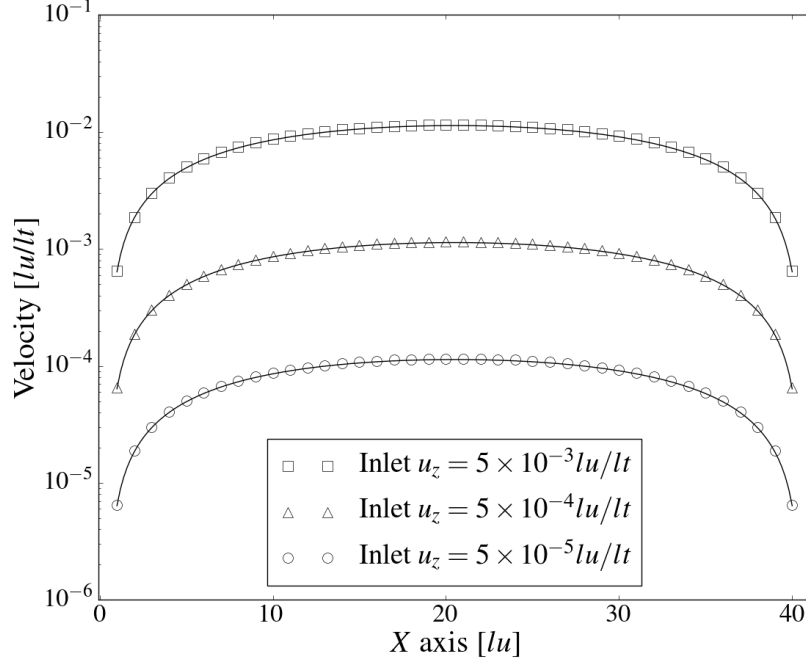


Figure 1: The velocity profiles for Poiseuille flow along the central line ($y = 20$ lu) at the middle plane of the square tube ($z = 40$ lu). The solid lines indicate the theoretical solutions given by Eq.10.

The proposed boundary condition was incorporated into the MRT LBM with the relaxation time chosen as $\tau = 1.0$. Three cases of inlet fluid velocity u_z were applied to the boundary, and Fig. 1 shows that the simulation results compared to the analytical solution given in Eq. 10. The numerical results are in close agreement with the analytical solutions, which validates the implementation for single-fluid flow.

3.2. Immiscible displacement at constant capillary number

The LBM is often used to simulate immiscible two-fluid displacement in porous media. We consider a typical experiment in which the following quantities are known:

1. Q_z the volumetric flow rate (e.g. in mL/min),

2. $L_x \times L_y \times L_z$ the physical dimensions of the sample (e.g. in mm),
3. ϵ the porosity of the sample,
4. μ_w, μ_n the dynamic viscosity for each fluid (e.g. in mPa · s), and
5. γ_{wn} the interfacial tension between fluids (e.g. mN/m).

To match experimental conditions with a simulation, physical quantities must be expressed in terms of the lattice length δx and the timestep δt . When the input geometry is provided from experimental micro-computed tomography (μ CT), the lattice spacing δx is determined based on the width of a voxel (i.e. the image resolution). The relationship for time is obtained by considering appropriate non-dimensional quantities and choosing the simulation parameters such that experimental conditions are met. For an experiment where one fluid is displacing another and compressibility effects are negligible, the flow rates for each fluid will satisfy

$$\frac{\partial s^w}{\partial t} = \frac{Q_z}{\epsilon V}, \quad (12)$$

where s^w is the wetting-phase saturation, and V is the total volume of the system. The conversion between the lattice timestep δt and physical units can therefore be determined based on the rate of change in saturation. Noting that this choice does not uniquely determine the parameters, for two-fluid flows it is desirable to match the capillary number,

$$\text{Ca} = \frac{\mu_w Q_z}{\gamma_{wn} \epsilon A}, \quad (13)$$

where A is the area of the inlet boundary Γ_i , and the mobility

$$\text{M} = \frac{\mu_w}{\mu_n}. \quad (14)$$

An additional constraint is obtained by choosing the simulated capillary number to match the experimental value,

$$Q_z^{sim} = \epsilon A^{sim} \frac{\gamma_{wn}^{sim}}{\mu_w^{sim}} \text{Ca}. \quad (15)$$

To reduce the number of time steps required, it is desirable to choose Q_z^{sim} to be as large as possible, since this will induce the largest change in saturation

per time step. At fixed Ca , this is accomplished when γ_{sim}/μ_{sim} is as large as possible. The values of γ_{sim} and μ_{sim} are constrained by numerical stability and the mobility; for the color-gradient based LBM used in this work [32], the stable range for fluid parameters explored was $1 \times 10^{-5} \leq \gamma_{wn}^{sim} \leq 1 \times 10^{-2}$, $1/15 \leq \nu_i \leq 1/3$ and $0.01 \leq \rho_i \leq 1.0$ for $i \in \{w, n\}$. As a general rule of thumb, LBMs tend to become unstable if flow velocity ($|\mathbf{u}|$) exceeds ~ 0.1 anywhere on the lattice. Combinations of parameters that create this situation can result numerical instability (since the LBM is an explicit method) and compressibility errors (since the continuum physics are only recovered in the limit of small Mach number) [37, 38].

3.2.1. Immiscible two-fluid displacement in a square tube

The proposed boundary condition was first investigated in a square tube where a drainage simulation was performed. The same tube size as in single-phase simulations was used. The computation domain consists of a capillary tube sandwiched by a non-wetting phase reservoir (NWR) and a wetting phase reservoir (WR), each with six layers of pure fluid nodes. For simplicity, unity density and viscosity ratios was used. Three cases of lattice volumetric flow rate, $Q_z^{sim} = \{0.02, 0.2, 2.0\} \text{ lu}^3/\text{lt}$, were simulated. As shown in Fig. 2, the time rate change of the saturation, $\partial s^w/\partial t$, multiplied by the pore volume of the tube (ϵV), is plotted (in blue) against different Q_z^{sim} . The color of the data points indicates the temporal evolution, with the time scale normalized by the total simulation time. It can be seen that, as time evolves, the time rate change of the saturation approaches the prescribed Q_z^{sim} once the steady state displacement is reached. It is also noted that at the initial stage $\partial s^w/\partial t$ deviates from Q_z^{sim} , but eventually stabilizes to match the to match the boundary flux. While the prescribed boundary flux will match exactly (since Eq. 9 is not approximate), fluctuations in $\partial s^w/\partial t$ are possible due to fluid compressibility and the rearrangement of the diffuse interface in the color LBM. At low flow rates the presence of spurious currents may influence the accuracy of the boundary condition, which is a known limitation of the color LBM. This can

be mitigated by using larger fluid reservoirs such that spurious currents do not arise in proximity to the boundary.

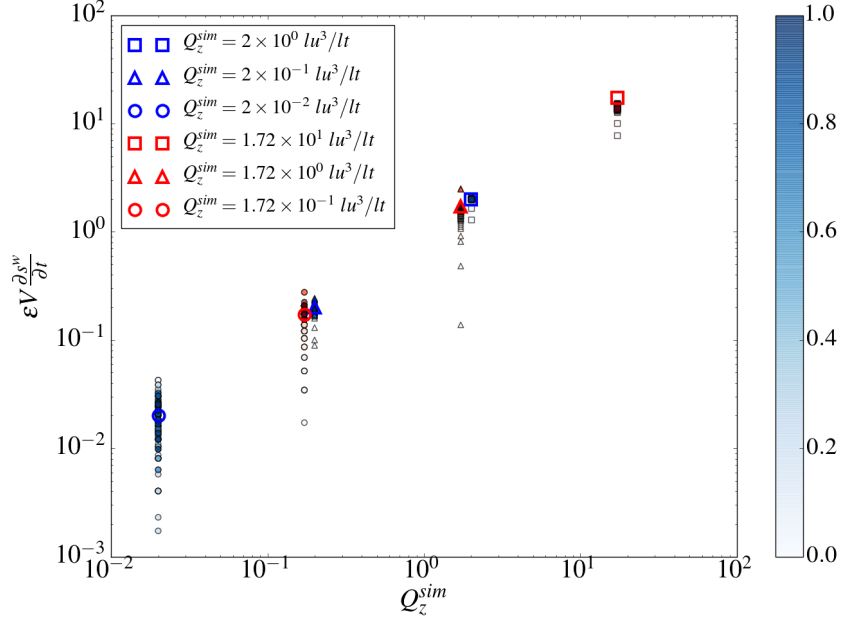


Figure 2: The time rate change of the saturation (scaled by the pore volume of the media) in the primary drainage simulations, is plotted against the volumetric flow rate Q_z^{sim} specified at the inlet, for the case of the square tube in blue, and for the case of the Bentheimer sandstone in red. The color of the data points indicates the temporal evolution, and the time scale is normalized by the total simulation time. For visual clarity only the color bar (in blue) for the square tube case is presented. The blank symbols are used to highlight the exact values of Q_z^{sim} . The lattice surface tension γ_{wn}^{sim} is 6×10^{-5} . The phase density ρ_i^{sim} is 1.0, and the phase kinematic viscosity ν_i^{sim} is 1/6 (i.e. $\tau_i = 1.0$), where $i \in \{w, n\}$.

3.2.2. Immiscible two-fluid displacement in a realistic porous medium

The proposed boundary condition was also tested with primary drainage simulations in an X-ray μ CT image of Bentheimer sandstone sample. A sub-domain of 256^3 lu^3 of the original image was used, with an image resolution of $4.95 \mu\text{m}/\text{lu}$ [39]. The sub-domain was again sandwiched by six layers of NWR and WR, respectively. Unity density and viscosity ratios were adopted. Three

cases of lattice volumetric flow rate, $Q_z^{sim} = \{0.172, 1.72, 17.2\} \text{ lu}^3/\text{lt}$ were set such that the capillary numbers were the same as in the square tube case. The corresponding time rate change of the saturation is also shown in Fig. 2 in red. Due to the initial capillary entry effect, the time rate change gradually approaches the prescribed Q_z^{sim} as the steady state displacement is reached. Moreover, to illustrate the capability of the proposed boundary condition to locally adjust the inlet flux, the two-dimensional $u_z(x, y)$ profile at the inlet boundary of NWR, for the case of $Q_z^{sim} = 1.72 \text{ lu}^3/\text{lt}$ is shown in Fig. 3. Since the NWR consists of pure fluid nodes, a contour line in white delineating the fluid-solid boundary of the first layer of the porous medium is also shown. It can be seen that the proposed boundary condition only directs positive flux towards the pore space of the medium, while maintaining zero flux for where the solid phase is present. This demonstrates that the boundary condition allows the local flow rate to vary across the boundary region based on the interior structure of the flow, while maintaining control over the volumetric flow rate for fluid injected into the system.

4. Conclusions

In this paper, we present a volumetric flux boundary condition for lattice Boltzmann methods. The approach is derived based on a consistency condition that is associated with a pressure boundary condition. By integrating the consistency condition over the relevant boundary region, a spatially-constant potential can be determined and enforced along that boundary to produce a desired volumetric flow rate. The local velocity can vary in time and space along the boundary depending on the interior flow dynamics, providing an advantage relative to the standard velocity boundary conditions used in conjunction with LBMs. The boundary condition is validated analytically for one-and two-fluid lattice Boltzmann schemes and applied to simulate two-fluid flow within an experimentally-obtained Bentheimer sandstone image. We delineate an approach to match experimental conditions for two-fluid flow based on the reso-

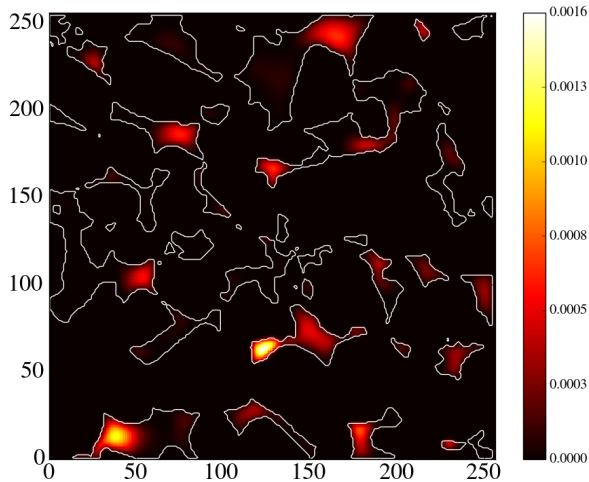


Figure 3: The cross-sectional view of the velocity field $u_z(x, y)$ at the inlet boundary of NWR in Bentheimer sandstone primary drainage simulation for the case of $Q_z^{sim} = 1.72 \text{ lu}^3/\text{lt}$. The white contour line depicts the fluid-solid boundary of the first layer of the medium. The velocity field was extracted at time step 250,000 lt when the steady state displacement was reached.

lution, volumetric flow rate, capillary number and viscosity ratio. For two-fluid simulations, spurious currents associated with the interfacial stresses can reduce the accuracy of the approach, although the method is sufficient to set the capillary number to match experimental conditions in practice. The boundary condition provides an attractive alternative to existing LBM boundary conditions for modeling flow experiments within porous media.

Appendix A: Momentum and mass transport in multiphase lattice-Boltzmann model

The multiphase “color” LBM used in this work is based on the implementation described in McClure *et al.* [32]. The momentum transport is modeled by

the lattice-Boltzmann equation (LBE) as:

$$f_q(\mathbf{x}_i + \boldsymbol{\xi}_q \delta t, t + \delta t) - f_q(\mathbf{x}_i, t) = \sum_{k=0}^{Q-1} M_{q,k}^{-1} S_{k,k} (m_k^{eq} - m_k),$$

where the transformation matrix $M_{q,k}$ (its inverse $M_{q,k}^{-1}$) maps the distribution function to its moments by $m_k = \sum_{q=0}^{Q-1} M_{q,k} f_q$, and diagonal matrix $S_{k,k}$ specifies the relaxation rates for each moment. For D3Q19 lattice structure, the $M_{q,k}$ can be found in [40], and the 19 moments are defined as:

$$\mathbf{m} = (\rho, e, \epsilon, j_x, q_x, j_y, q_y, j_z, q_z, 3p_{xx}, 3\pi_{xx}, p_{ww}, \pi_{ww}, p_{xy}, p_{yz}, p_{zx}, m_x, m_y, m_z),$$

These 19 moments $\{m_k \mid k = 0, 1, \dots, 18\}$ are the mass density ($m_0 = \rho$), the part of the kinetic energy independent of the density ($m_1 = e$), the part of the kinetic energy square independent of the density and kinetic energy ($m_2 = \epsilon = e^2$), the momentum flux ($m_{3,5,7} = j_{x,y,z}$), the energy flux ($m_{4,6,8} = q_{x,y,z}$), the symmetric traceless viscous stress tensor ($m_9 = 3p_{xx}$, $m_{11} = p_{ww}$, and $m_{13,14,15} = p_{xy,yz,zx}$), the vectors of quartic order ($m_{10} = 3\pi_{xx}$, $m_{12} = \pi_{ww}$), and the vectors of cubic order ($m_{16,17,18} = m_{x,y,z}$) [40]. The relaxation rates for each moment are given by:

$$\mathbf{S} = \text{diag}(0, s_e, s_\epsilon, 0, s_q, 0, s_q, 0, s_q, s_\nu, s_\pi, s_\nu, s_\pi, s_\nu, s_\nu, s_\nu, s_m, s_m, s_m),$$

where, the relaxation rates for the conserved moments, the density ρ and the momentum (j_x, j_y, j_z), are set to zero, since they are not affected by collisions. Following the reported work in [41], the relaxation rates for the non-conserved moments are set as

$$s_e = s_\epsilon = s_\pi = s_\nu, \quad s_q = s_m = 8 \frac{(2 - s_\nu)}{(8 - s_\nu)}.$$

The fluid kinetic viscosity ν is given by:

$$\nu = c_s^2 \left(\frac{1}{s_\nu} - \frac{1}{2} \right),$$

and in the main text, the commonly used relaxation time τ is defined as $\tau = s_\nu^{-1}$.

In the case of multiphase flow, the equilibrium moments m_q^{eq} are set such that the stress tensor matches that of a Newtonian fluid with an anisotropic

contribution due to the interfacial tension. Following McClure *et al.*, the non-zero equilibrium moments are given by: [32]

$$\begin{aligned}
m_1^{eq} &= (j_x^2 + j_y^2 + j_z^2) + \alpha |\mathbf{C}| \\
m_9^{eq} &= (2j_x^2 - j_y^2 - j_z^2) + \alpha \frac{|\mathbf{C}|}{2} (2n_x^2 - n_y^2 - n_z^2) \\
m_{11}^{eq} &= (j_y^2 - j_z^2) + \alpha \frac{|\mathbf{C}|}{2} (n_y^2 - n_z^2) \\
m_{13}^{eq} &= j_x j_y + \alpha \frac{|\mathbf{C}|}{2} n_x n_y \\
m_{14}^{eq} &= j_y j_z + \alpha \frac{|\mathbf{C}|}{2} n_y n_z \\
m_{15}^{eq} &= j_x j_z + \alpha \frac{|\mathbf{C}|}{2} n_x n_z ,
\end{aligned}$$

where the parameter α is linearly related to the interfacial tension, and \mathbf{C} is the color gradient, which is defined as the gradient of the phase field:

$$\mathbf{C} = \nabla \varphi ,$$

where the phase field φ is defined based on the densities of the non-wetting and wetting fluids, ρ_n and ρ_w , respectively, which is given by:

$$\varphi = \frac{\rho_n - \rho_w}{\rho_n + \rho_w} .$$

$\mathbf{n} = (n_x, n_y, n_z)$ is the unit normal vector of the color gradient and is calculated as:

$$\mathbf{n} = \frac{\mathbf{C}}{|\mathbf{C}|} .$$

The phase indicator field is tracked by solving two additional mass transport LBEs that rely on the three-dimensional, seven velocity model (D3Q7). The seven velocities for the D3Q7 model correspond to $q = 0, 1, \dots, 6$ in the D3Q19 model. D3Q7 distributions model the evolution of the number density of each fluid, N_A and N_B , respectively, which are given by

$$N_A = \sum_{q=0}^6 A_q , \quad N_B = \sum_{q=0}^6 B_q , \quad \text{and } \phi = \frac{N_A - N_B}{N_A + N_B} . \quad (16)$$

The distributions are updated based on

$$A_q(\mathbf{x} + \boldsymbol{\xi}_q \delta t, t + \delta t) = w_q N_A \left[1 + \frac{9}{2} \mathbf{u} \cdot \boldsymbol{\xi}_q + \beta N_B \mathbf{n} \cdot \boldsymbol{\xi}_q \right] \text{ and} \quad (17)$$

$$B_q(\mathbf{x} + \boldsymbol{\xi}_q \delta t, t + \delta t) = w_q N_B \left[1 + \frac{9}{2} \mathbf{u} \cdot \boldsymbol{\xi}_q - \beta N_A \mathbf{n} \cdot \boldsymbol{\xi}_q \right], \quad (18)$$

where β controls the interface width, $w_0 = 1/3$ and $w_{1,\dots,6} = 1/9$. The mass transport LBEs ensure phase separation based on the color gradient, which then couples to the momentum transport.

Appendix B: Pressure Boundary Condition for D3Q19

At the inlet, the unknown distributions are $f_5, f_{11}, f_{14}, f_{15}$ and f_{18} . The above expressions can be rearranged to place the unknowns on the left-hand side:

$$\begin{aligned} f_5 + f_{11} + f_{14} + f_{15} + f_{18} &= \rho - (f_0 + f_1 + f_2 + f_3 + f_4 + f_6 + f_7 + \\ &\quad f_8 + f_9 + f_{10} + f_{12} + f_{13} + f_{16} + f_{17}) \\ f_{11} - f_{14} &= \rho_0 u_x - (f_1 - f_2 + f_7 - f_8 + f_9 - f_{10} - f_{12} + f_{13}) \\ f_{15} - f_{18} &= \rho_0 u_y - (f_3 - f_4 + f_7 - f_8 - f_9 + f_{10} - f_{16} + f_{17}) \\ f_5 + f_{11} + f_{14} + f_{15} + f_{18} &= \rho_0 u_z + (f_6 + f_{12} + f_{13} + f_{16} + f_{17}). \end{aligned}$$

It is clear that the sum $f_5 + f_{11} + f_{14} + f_{15} + f_{18}$ is determined either by choosing ρ or by choosing $\rho_0 u_z$; both conditions cannot be set independently. If a pressure boundary condition is use to determine ρ , then a consistency condition can be established by eliminating the sum of the unknowns from

$$\begin{aligned} \rho - (f_0 + f_1 + f_2 + f_3 + f_4 + f_6 + f_7 + f_8 + f_9 + f_{10} + f_{12} + f_{13} + f_{16} + f_{17}) &= \\ \rho_0 u_z - (-f_6 - f_{12} - f_{13} - f_{16} - f_{17}), &\quad (19) \end{aligned}$$

which can then be solved to determine the associated velocity

$$u_z = \frac{\rho}{\rho_0} - \frac{1}{\rho_0} [f_0 + f_1 + f_2 + f_3 + f_4 + f_7 + f_8 + f_9 + f_{10} + 2(f_6 + f_{12} + f_{13} + f_{16} + f_{17})]. \quad (20)$$

The equilibrium distributions for the D3Q19 model are

$$f_q^{eq}(\rho, \mathbf{u}) = w_i \left[\rho + \rho_0 \left(3\xi_q \cdot \mathbf{u} + \frac{9}{2} (\xi_q \cdot \mathbf{u})^2 + \frac{3}{2} \mathbf{u} \cdot \mathbf{u} \right) \right]. \quad (21)$$

With both ρ and \mathbf{u} known, the unknown distributions are chosen by assuming that the bounce-back rule applies to the non-equilibrium part of the unknown distributions, for example:

$$f_q - f_q^{eq} = f_{\bar{q}} - f_{\bar{q}}^{eq}, \quad (22)$$

where $\xi_q = -\xi_{\bar{q}}$. This can be solved for the unknown distribution

$$f_q = f_{\bar{q}} + f_q^{eq} - f_{\bar{q}}^{eq} \quad (23)$$

$$= f_{\bar{q}} + 6\rho_0 w_i (\xi_q \cdot \mathbf{u}), \quad (24)$$

where the definition of the equilibrium distributions has been inserted, using the fact that $\xi_q = -\xi_{\bar{q}}$. This is used to determine

$$f_5 = f_6 + \frac{1}{3} \rho_0 u_z.$$

This leaves four remaining unknowns and only three equations. Hecht and Harding resolve the closure problem by defining

$$N_x^z = \frac{1}{2} [f_1 + f_7 + f_9 - (f_2 + f_{10} + f_8)] - \frac{1}{3} \rho_0 u_x \quad (25)$$

$$N_y^z = \frac{1}{2} [f_3 + f_7 + f_{10} - (f_4 + f_9 + f_8)] - \frac{1}{3} \rho_0 u_y, \quad (26)$$

and then providing a closed system based on the equations

$$f_{11} - f_{11}^{eq} = f_{12} - f_{12}^{eq} - N_x^z \quad (27)$$

$$f_{14} - f_{14}^{eq} = f_{13} - f_{13}^{eq} - N_x^z \quad (28)$$

$$f_{15} - f_{15}^{eq} = f_{16} - f_{16}^{eq} - N_x^z \quad (29)$$

$$f_{18} - f_{18}^{eq} = f_{17} - f_{17}^{eq} - N_x^z, \quad (30)$$

which can be simplified to the form

$$f_{11} - f_{12} = \frac{1}{6}\rho_0(u_x + u_z) - N_x^z \quad (31)$$

$$f_{14} - f_{13} = \frac{1}{6}\rho_0(-u_x + u_z) + N_x^z \quad (32)$$

$$f_{15} - f_{16} = \frac{1}{6}\rho_0(u_y + u_z) - N_y^z \quad (33)$$

$$f_{18} - f_{17} = \frac{1}{6}\rho_0(-u_y + u_z) + N_y^z . \quad (34)$$

These expressions can be rearranged to solve for the unknown distributions for either the inlet or outlet.

Acknowledgements

This work was supported by Army Research Office grant W911NF-14-1-02877 and National Science Foundation grant 1619767. An award of computer time was provided by the Department of Energy INCITE program. This research also used resources of the Oak Ridge Leadership Computing Facility, which is a DOE Office of Science User Facility supported under Contract DE-AC05-00OR22725. Z.L. acknowledges the Australian Government Research Training Program (RTP) Scholarship and the Robert and Helen Crompton travel fund. A.P.S. acknowledges the support of an Australian Research Council Future Fellowship through project FT100100470. This research also used resources and services from the National Computational Infrastructure (NCI), which is supported by the Australian Government.

References

References

- [1] T. Colonius, Modeling artificial boundary conditions for compressible flow, *Annual Review of Fluid Mechanics* 36 (2004) 315–345. doi:{10.1146/annurev.fluid.36.050802.121930}.

- [2] S. Leclaire, M. Reggio, J.-Y. Trepanier, Progress and investigation on lattice Boltzmann modeling of multiple immiscible fluids or components with variable density and viscosity ratios, *Journal of Computational Physics* 246 (2013) 318–342. doi:{10.1016/j.jcp.2013.03.039}.
- [3] Q. Kang, L. Chen, A. J. Valocchi, H. S. Viswanathan, Pore-scale study of dissolution-induced changes in permeability and porosity of porous media, *Journal of Hydrology* 517 (2014) 1049–1055. doi:{10.1016/j.jhydrol.2014.06.045}.
- [4] L. Chen, Q. Kang, B. Carey, W.-Q. Tao, Pore-scale study of diffusion-reaction processes involving dissolution and precipitation using the lattice Boltzmann method, *International Journal of Heat and Mass Transfer* 75 (2014) 483–496. doi:{10.1016/j.ijheatmasstransfer.2014.03.074}.
- [5] H. Liu, A. J. Valocchi, Y. Zhang, Q. Kang, Phase-field-based lattice Boltzmann finite-difference model for simulating thermocapillary flows, *Physical Review E* 87 (1). doi:{10.1103/PhysRevE.87.013010}.
- [6] T. Ramstad, N. Idowu, C. Nardi, P.-E. Oren, Relative permeability calculations from two-phase flow simulations directly on digital images of porous rocks, *Transport in Porous Media* 94 (2, SI) (2012) 487–504.
- [7] M. L. Porter, E. T. Coon, Q. Kang, J. D. Moulton, J. W. Carey, Multi-component interparticle-potential lattice Boltzmann model for fluids with large viscosity ratios, *Physical Review E* 86 (3, Part 2).
- [8] B. Ahrenholz, J. Tölke, P. Lehmann, A. Peters, A. Kaestner, M. Krafczyk, W. Durner, Prediction of capillary hysteresis in a porous material using lattice-boltzmann methods and comparisons to experimental data and morphological pore network model, *Advances in Water Resources* 31 (9) (2008) 1151–1173.
- [9] Q. Lou, Z. Guo, B. Shi, Evaluation of outflow boundary conditions for

- two-phase lattice Boltzmann equation, *Physical Review E* 87 (6). doi:
{10.1103/PhysRevE.87.063301}.
- [10] R. Maier, R. Bernard, D. Grunau, Boundary conditions for the lattice Boltzmann method, *Physics of Fluids* 8 (7) (1996) 1788–1801. doi:{10.1063/1.868961}.
- [11] D. d’Humières, P. Lallemand, U. Frisch, Lattice gas models for 3d hydrodynamics, *EPL (Europhysics Letters)* 2 (4) (1986) 291.
URL <http://stacks.iop.org/0295-5075/2/i=4/a=006>
- [12] Y. H. Qian, D. D’Humières, P. Lallemand, Lattice bgk models for navier-stokes equation, *EPL (Europhysics Letters)* 17 (6) (1992) 479.
URL <http://stacks.iop.org/0295-5075/17/i=6/a=001>
- [13] S. Chen, D. O. Martínez, W. H. Matthaeus, H. Chen, Magneto-hydrodynamics computations with lattice gas automata, *Journal of Statistical Physics* 68 (3) (1992) 533–556. doi:10.1007/BF01341761.
URL <https://doi.org/10.1007/BF01341761>
- [14] D. d’Humières, M. Bouzidi, P. Lallemand, Thirteen-velocity three-dimensional lattice boltzmann model, *Phys. Rev. E* 63 (2001) 066702. doi:10.1103/PhysRevE.63.066702.
URL <https://link.aps.org/doi/10.1103/PhysRevE.63.066702>
- [15] R. Benzi, S. Succi, M. Vergassola, The lattice boltzmann equation: theory and applications, *Physics Reports* 222 (3) (1992) 145 – 197. doi:[https://doi.org/10.1016/0370-1573\(92\)90090-M](https://doi.org/10.1016/0370-1573(92)90090-M).
URL <http://www.sciencedirect.com/science/article/pii/037015739290090M>
- [16] S. Chen, G. D. Doolen, Lattice boltzmann method for fluid flows, *Annual Review of Fluid Mechanics* 30 (1) (1998) 329–364. arXiv:<https://doi.org/10.1146/annurev.fluid.30.1.329>, doi:10.1146/annurev.

fluid.30.1.329.

URL <https://doi.org/10.1146/annurev.fluid.30.1.329>

- [17] A. K. Gunstensen, D. H. Rothman, S. Zaleski, G. Zanetti, Lattice boltzmann model of immiscible fluids, *Phys. Rev. A* 43 (1991) 4320–4327. doi:10.1103/PhysRevA.43.4320.

URL <https://link.aps.org/doi/10.1103/PhysRevA.43.4320>

- [18] X. Shan, H. Chen, Lattice boltzmann model for simulating flows with multiple phases and components, *Phys. Rev. E* 47 (1993) 1815–1819. doi:10.1103/PhysRevE.47.1815.

URL <https://link.aps.org/doi/10.1103/PhysRevE.47.1815>

- [19] M. R. Swift, W. R. Osborn, J. M. Yeomans, Lattice boltzmann simulation of nonideal fluids, *Phys. Rev. Lett.* 75 (1995) 830–833. doi:10.1103/PhysRevLett.75.830.

URL <https://link.aps.org/doi/10.1103/PhysRevLett.75.830>

- [20] X. He, S. Chen, R. Zhang, A lattice boltzmann scheme for incompressible multiphase flow and its application in simulation of Rayleigh-Taylor instability, *Journal of Computational Physics* 152 (2) (1999) 642 – 663. doi:<https://doi.org/10.1006/jcph.1999.6257>.

URL <http://www.sciencedirect.com/science/article/pii/S0021999199962575>

- [21] T. Lee, L. Liu, Lattice boltzmann simulations of micron-scale drop impact on dry surfaces, *Journal of Computational Physics* 229 (20) (2010) 8045 – 8063. doi:<https://doi.org/10.1016/j.jcp.2010.07.007>.

URL <http://www.sciencedirect.com/science/article/pii/S0021999110003761>

- [22] X. Shan, Simulation of Rayleigh-Bénard convection using a lattice boltzmann method, *Phys. Rev. E* 55 (1997) 2780–2788. doi:10.1103/PhysRevE.55.2780.

URL <https://link.aps.org/doi/10.1103/PhysRevE.55.2780>

- [23] X. He, S. Chen, G. D. Doolen, A novel thermal model for the lattice boltzmann method in incompressible limit, *Journal of Computational Physics* 146 (1) (1998) 282 – 300. doi:<https://doi.org/10.1006/jcph.1998.6057>.
URL <http://www.sciencedirect.com/science/article/pii/S0021999198960570>
- [24] P. Lallemand, L.-S. Luo, Theory of the lattice boltzmann method: Acoustic and thermal properties in two and three dimensions, *Phys. Rev. E* 68 (2003) 036706. doi:[10.1103/PhysRevE.68.036706](https://doi.org/10.1103/PhysRevE.68.036706).
URL <https://link.aps.org/doi/10.1103/PhysRevE.68.036706>
- [25] L. Li, R. Mei, J. F. Klausner, Boundary conditions for thermal lattice Boltzmann equation method, *Journal of Computational Physics* 237 (2013) 366–395. doi:[10.1016/j.jcp.2012.11.027](https://doi.org/10.1016/j.jcp.2012.11.027).
- [26] S. P. Dawson, S. Chen, G. D. Doolen, Lattice boltzmann computations for reaction-diffusion equations, *The Journal of Chemical Physics* 98 (2) (1993) 1514–1523. arXiv:<https://doi.org/10.1063/1.464316>, doi:[10.1063/1.464316](https://doi.org/10.1063/1.464316).
URL <https://doi.org/10.1063/1.464316>
- [27] D. Wolf-Gladrow, A lattice boltzmann equation for diffusion, *Journal of Statistical Physics* 79 (5) (1995) 1023–1032. doi:[10.1007/BF02181215](https://doi.org/10.1007/BF02181215).
URL <https://doi.org/10.1007/BF02181215>
- [28] R. van der Sman, M. Ernst, Convection-diffusion lattice boltzmann scheme for irregular lattices, *Journal of Computational Physics* 160 (2) (2000) 766 – 782. doi:<https://doi.org/10.1006/jcph.2000.6491>.
URL <http://www.sciencedirect.com/science/article/pii/S002199910096491X>
- [29] X. Zhang, A. G. Bengough, L. K. Deeks, J. W. Crawford, I. M. Young, A novel three-dimensional lattice boltzmann model for solute transport in

variably saturated porous media, *Water Resources Research* 38 (9) (2002) 6–1–6–10, 1167. doi:10.1029/2001WR000982.

URL <http://dx.doi.org/10.1029/2001WR000982>

- [30] F. Verhaeghe, S. Arnout, B. Blanpain, P. Wollants, Lattice-boltzmann modeling of dissolution phenomena, *Phys. Rev. E* 73 (2006) 036316. doi:10.1103/PhysRevE.73.036316.

URL <https://link.aps.org/doi/10.1103/PhysRevE.73.036316>

- [31] Q. Kang, P. C. Lichtner, D. Zhang, An improved lattice boltzmann model for multicomponent reactive transport in porous media at the pore scale, *Water Resources Research* 43 (12) (2007) n/a–n/a, w12S14. doi:10.1029/2006WR005551.

URL <http://dx.doi.org/10.1029/2006WR005551>

- [32] J. McClure, J. Prins, C. Miller, A novel heterogeneous algorithm to simulate multiphase flow in porous media on multicore CPU-GPU systems, *Computer Physics Communications* 185 (7) (2014) 1865 – 1874. doi:<https://doi.org/10.1016/j.cpc.2014.03.012>.

URL <http://www.sciencedirect.com/science/article/pii/S0010465514000927>

- [33] C. Pan, L.-S. Luo, C. T. Miller, An evaluation of lattice boltzmann schemes for porous medium flow simulation, *Computers & Fluids* 35 (8) (2006) 898 – 909, proceedings of the First International Conference for Mesoscopic Methods in Engineering and Science. doi:<https://doi.org/10.1016/j.compfluid.2005.03.008>.

URL <http://www.sciencedirect.com/science/article/pii/S0045793005001520>

- [34] Q. Zou, X. He, On pressure and velocity boundary conditions for the lattice Boltzmann BGK model, *Physics of Fluids* 9 (6) (1997) 1591–1598. doi:{10.1063/1.869307}.

- [35] M. Hecht, J. Harting, Implementation of on-site velocity boundary conditions for D3Q19 lattice Boltzmann simulations, *Journal of Statistical Mechanics: Theory and Experiment* 1 (2010) 01018. doi:10.1088/1742-5468/2010/01/P01018.
- [36] W. Zhang, B. Shi, Y. Wang, 14-velocity and 18-velocity multiple-relaxation-time lattice boltzmann models for three-dimensional incompressible flows, *Computers & Mathematics with Applications* 69 (9) (2015) 997 – 1019. doi:<https://doi.org/10.1016/j.camwa.2015.03.001>.
URL <http://www.sciencedirect.com/science/article/pii/S0898122115000966>
- [37] J. Sterling, S. Chen, Stability analysis of lattice boltzmann methods, *Journal of Computational Physics* 123 (1) (1996) 196 – 206. doi:<https://doi.org/10.1006/jcph.1996.0016>.
URL <http://www.sciencedirect.com/science/article/pii/S0021999196900169>
- [38] M. Junk, A. Klar, L.-S. Luo, Asymptotic analysis of the lattice boltzmann method, *Journal of Computational Physics* 210 (2005) 676–704.
- [39] A. L. Herring, J. Middleton, R. Walsh, A. Kingston, A. Sheppard, Flow rate impacts on capillary pressure and interface curvature of connected and disconnected fluid phases during multiphase flow in sandstone, *Advances in Water Resources* 107 (2017) 460 – 469. doi:<https://doi.org/10.1016/j.advwatres.2017.05.011>.
URL <http://www.sciencedirect.com/science/article/pii/S0309170816307011>
- [40] D. d’Humières, I. Ginzburg, M. Krafczyk, P. Lallemand, L.-S. Luo, Multiple-relaxation-time lattice boltzmann models in three dimensions, *Philosophical Transactions of the Royal Society of London A: Mathematical, Physical and Engineering Sciences* 360 (1792) (2002) 437–451. arXiv:<http://rsta.royalsocietypublishing.org/content/360/>

1792/437.full.pdf, doi:10.1098/rsta.2001.0955.

URL <http://rsta.royalsocietypublishing.org/content/360/1792/437>

- [41] I. Ginzburg, D. d'Humières, Multireflection boundary conditions for lattice boltzmann models, Phys. Rev. E 68 (2003) 066614. doi:10.1103/PhysRevE.68.066614.

URL <https://link.aps.org/doi/10.1103/PhysRevE.68.066614>